ALETHEIA
Alpha Chi's Journal of Undergraduate Scholarship
Volume 10 | 2025

Investigating the structure of phosphatidylinositol 3,4,5-triphosphate and phosphatidylinositol 4,5-bisphosphate under Transmission Electron Microscopy and X-ray crystallography

Mong Na Claire Loi

Vanderbilt University

***Aletheia* Vol. 10, 2025**
Title: Investigating the structure of phosphatidylinositol 3,4,5-triphosphate and phosphatidylinositol 4,5-bisphosphate under Transmission Electron Microscopy and X-ray crystallography
DOI: 10.21081/ax0404
ISSN: 2381-800X
Keywords: human liver receptor homolog-1 (hLRH-1), NR5A2 gene, fluorescently labeled lipid, rhodamine phosphoethanolamine (Rh-PE), 1,2-dilauroyl-sn-glycero-3-phosphocholine (DLPC), binding structure, X-ray crystallography, phospholipids

Volume 10 | 2025

Title: Investigating the structure of phosphatidylinositol 3,4,5-triphosphate and phosphatidylinositol 4,5-bisphosphate under Transmission Electron Microscopy and X-ray crystallography
DOI: 10.21081/ax0404
ISSN: 2381-800X

Investigating the structure of phosphatidylinositol 3,4,5-triphosphate and phosphatidylinositol 4,5-bisphosphate under Transmission Electron Microscopy and X-ray crystallography

Mong Na Claire Loi

Vanderbilt University

Abstract

Human liver receptor homolog-1 (hLRH-1), an orphan nuclear receptor coded by the NR5A2 gene, is crucial in regulating the balance of lipids, glucose, and cholesterol homeostasis. Previous studies have shown how the hLRH-1 ligand-binding domain (hLRH-1 LBD) binds phosphatidylinositol 3,4,5-triphosphate (PIP3) and phosphatidylinositol 4,5-bisphosphate (PIP2). However, whether the DNA-binding domain (DBD) and the LBD interact with each other in the full-length hLRH-1 when it is bound to PIP3 or PIP2 is still up for discussion. In this study, the structural interaction between the DBD and the LBD in full-length (FL) hLRH-1 when bound to PIP3 or PIP2 is examined. Considering the structure size, the PIP3 antibody (PIP3 AB) and PIP2 antibody (PIP2 AB) will be used. We hypothesize that the structures of PIP3 AB and PIP2 AB should be pentamers, and hLRH-1 will bind to all five on the outside, similar to a flower shape. Thus, the objective of this pilot experiment is to verify this hypothesis by examining the structure of PIP3 AB and PIP2 AB, involving protein purification, TEM imaging, X-ray crystallography, and co-incubation experiments, which provide a comprehensive approach to studying the interaction between hLRH-1 proteins and phosphatidylinositol antibodies. The results from these experiments will contribute to our understanding of the molecular mechanisms governing LRH-1 interaction with PIP3 and PIP2, potentially elucidating new insights into their functional roles and implications for therapeutic targeting.

Keywords: *human liver receptor homolog-1 (hLRH-1), NR5A2 gene, fluorescently labeled lipid, rhodamine phosphoethanolamine (Rh-PE), 1,2-dilauroyl-sn-glycero-3-phosphocholine (DLPC), binding structure, X-ray crystallography, phospholipids*

Introduction

Phosphoinositides (PIPs) are lipid signaling molecules that play key roles in signal transduction, membrane trafficking, and cytoskeletal organization. Among them, phosphatidylinositol 3-phosphate (PIP3) and phosphatidylinositol 3,4-bisphosphate (PIP2) are critical regulators of signaling pathways that govern cell growth, development, and metabolism.

Liver receptor homolog-1 (hLRH-1), a member of the nuclear receptor superfamily, has been identified as a major transcription factor that regulates genes involved in lipid metabolism, bile acid production, and steroidogenesis. hLRH-1 has been linked to a variety of physiological processes, highlighting its significance as a potential therapeutic target for metabolic disorders and hormone-related diseases. Recent studies have suggested a possible interaction between hLRH-1 and phosphatidylinositol antibodies, particularly PIP3AB and PIP2AB. These antibodies, designed to target PIP3 and PIP2, respectively, may play a regulatory role in modulating hLRH-1 activity through direct binding interactions.

Understanding the structural basis of hLRH-1's interaction with PIP3AB and PIP2AB could provide valuable insights into the molecular mechanisms underlying LRH-1 signaling and its implications for health and disease. Hence, in this study, the binding interaction between hLRH-1 and the phosphatidylinositol antibodies PIP3AB and PIP2AB was investigated to elucidate their structural arrangement and potential functional consequences. A combination of protein purification, transmission electron microscopy (TEM) imaging, X-ray crystallography, and co-incubation experiments was employed to characterize the complex formation between hLRH-1 and PIP3/PIP2 antibodies and to explore their roles in mediating cellular signaling pathways.

Once the hLRH–1–ligand–bound structure was solved by X-ray crystallography, it served as a seeding or soaking target crystal for subsequent experiments. Seeding allowed the bypass of the nucleation step and directly facilitated crystal development, as crystal growth is a gradual accumulation of solution-state molecules onto a nascent crystal. Similarly, crystal soaking enabled structural modifications by allowing the ligand to interact with the protein in solution before crystal lattice formation. In this process, pre-grown crystals were soaked with the molecule of interest. However, due to limitations in the crystal growth process, TEM was primarily used to validate the topology and structure of the ligand-bound complex. TEM imaging also assisted in confirming the binding interaction between LRH-1 and PIP3/PIP2 antibodies. This approach enabled visualization of the complex formation at the molecular level and provided insights into the spatial arrangement of the components involved in the interaction. A structural reference for hLRH-1 bound to PIP3 and its co-regulator is shown in Figure 1, which provides context for the molecular interaction explored in this study.

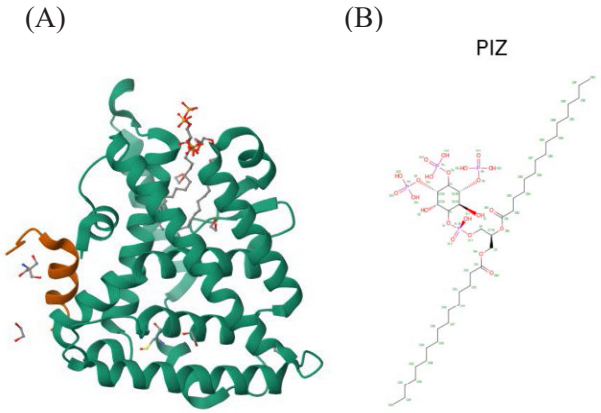

Figure 1. DATA from RCSB PDB.
(A) Crystal structure of PIP3-bound human nuclear receptor hLRH-1 in complex with a co-regulator DAX-1 (NR0B1) peptide at 1.86 A resolution. (B) Molecule 3 is (2S)-3-{[(R)-{[(1S,2S,3R,4S,5S,6S)-2,6-dihydroxy-3,4,5-tris(phosphonooxy)cyclohexyl]oxy}(hydroxy) phosphoryl]oxy}propane -1,2-diyl dihexadecanoate (three-letter code: PIZ) (formula: C41H82O22P4).

Methods and Results

Protein Expression and Purification

The FL hLRH-1 gene was cloned into a pET28a expression vector with a His-tag for purification. It was necessary to transform the plasmid into BL21(DE3) *E. coli* cells for protein production. For initial culture, 50 µg/mL of ampicillin and a single colony were added to 50 mL of terrific medium and incubated overnight at 37 °C with shaking at 200 rpm. The overnight culture was then used to inoculate 1 L of terrific medium containing 50 µg/mL ampicillin, starting at an OD_{600} of 0.05. The culture was grown at 37 °C and 200 rpm until the OD_{600} reached 0.6–0.8, at which point protein expression was induced with 0.5 mM IPTG. After 4 additional hours of growth, cells were harvested by centrifugation

at 4,000 × g for 10 minutes at 4 °C. The cell pellet was resuspended in the lysis buffer (HEPES-based). The cells were lysed using 70% sonication on ice (10 seconds on, 20 seconds off) for a total of 5 minutes. The lysate was then centrifuged at 15,000 × g for 30 minutes at 4 °C to remove cellular debris. Since X-ray crystallography requires ultrapure samples (purity > 95%), it was necessary to cleave the 6×His-tag from hLRH-1. The His-tagged protein was purified again using a cobalt-IMAC column, such as HiTrap TALON crude or HisTrap HP. A binding buffer was used to wash out unbound protein, and the eluted protein was dialyzed overnight at 4 °C against QA buffer. A complete schematic of this workflow is shown in Figure 2, which summarizes all steps from gene cloning to final protein dialysis.

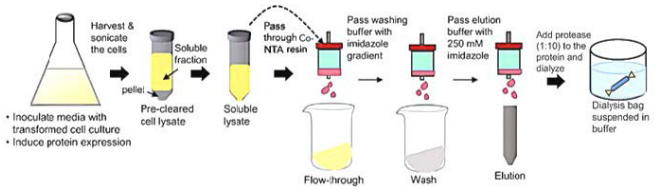

Figure 2. Protein expression and purification flow chart.

SDS-PAGE and Coomassie staining were then used to evaluate protein purity (Figure 3) and confirm successful cleavage of the 6×His-tag. The SDS-PAGE results indicated that the sample achieved ~98% purity and that the His-tag was successfully removed. The purified protein was aliquoted and stored at −80 °C until use (Note: For X-ray crystallography, hLRH-1 LBD must be ultrapure with >98% purity).

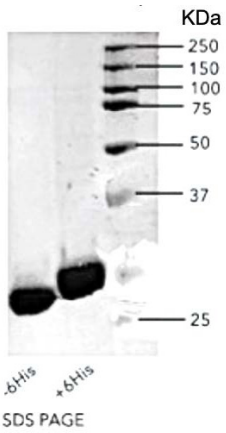

Figure 3. SDS-PAGE of FL hLRH1 sample with and without the 6 His-tag.

Negative Staining and Imaging Conditions

PIP3 AB and PIP2 AB samples were diluted at ratios of 1:10, 1:50, and 1:100 and desalted using a Zeba column. Uranyl formate (0.7% w/v) was protected from light during preparation. To dissolve the stain, 5 mL of boiling H_2O was added and stirred for 5 minutes. Next, 5 µL of 5 M NaOH was added (solution should turn a darker yellow), followed by an additional 5 minutes of stirring. Grids were glow discharged to restore hydrophilicity. The grid was placed on a glass slide in the glow discharger, and the process was run for ~45 seconds to 1 minute.

Parafilm, filter paper, H_2O, and stain were prepared in advance. Grids were held at the edge with the carbon side facing up. Two drops (30–40 µL each) of H_2O and stain were pipetted onto parafilm. 3–5 µL of the sample was applied and incubated for 30–60 seconds. Excess sample was blotted, and the grid was quickly washed in H_2O (5–10 seconds), blotted twice, and then washed again in stain. The grid was placed in a second stain drop for 1–1.5 minutes, blotted, and vacuum dried.

Stained samples were imaged under low magnification using a 50× objective lens. A detailed schematic of the negative staining process is provided in Figure 4. Condenser centering, focus adjustment via Fresnel fringes, and optimized contrast settings were applied to visualize protein structures.

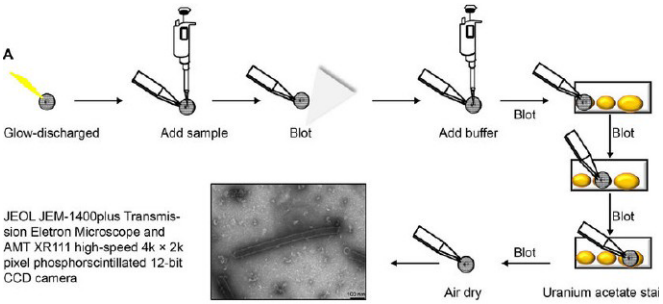

Figure 4. Schematic diagram of negative staining sample preparation. Scale bar: 100 nm. Adapted from Wang et al., 2021 (STAR Protoc. 3(1):101030), with modifications.

X-ray Crystallography

The general procedure for protein structure determination by X-ray crystallography is presented in Figure 5. After purification and crystallization, crystals were mounted on a goniometer and exposed to an X-ray beam. As the crystal rotated, diffraction patterns were recorded. The data were processed to extract X-ray intensities and positions. The phase problem was solved using direct methods or molecular replacement. A model of the atomic structure was then constructed using the experimental data.

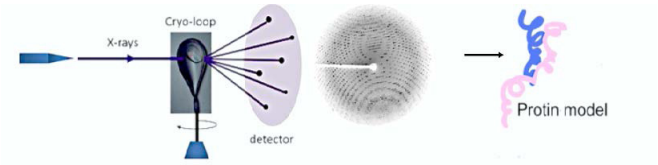

Figure 5. X-ray crystallography flow chart.

Computational Docking

Molecular docking simulations were conducted using AutoDock to predict binding modes and affinities between the protein and ligand molecules. The protein structure was prepared by removing water molecules and adding any missing atoms. Docking parameters were set, and multiple poses were generated and analyzed to determine potential binding sites and key interactions. Molecular docking simulations were conducted using AutoDock to predict binding modes and affinities between the protein and ligand molecules. The protein structure was prepared by removing water molecules and adding any missing atoms. Docking parameters were set, and multiple poses were generated and analyzed to determine potential binding sites and key interactions.

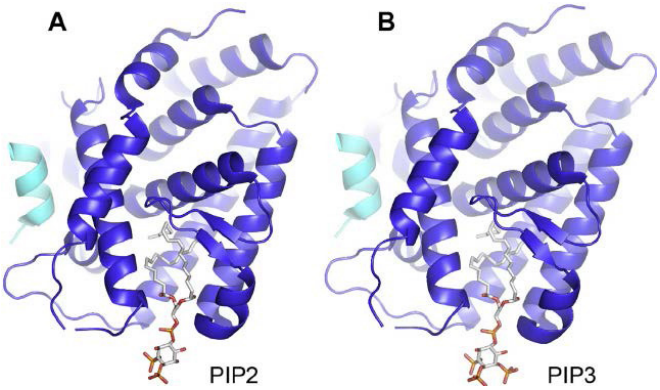

Figure 6. Structural similarity between steroidogenic factor-1 (SF-1) and liver receptor homolog-1 (LRH-1) based on docking simulations. (A) SF-1/PIP2. (B) SF-1/PIP3. These results suggest that PIP2 AB and PIP3 AB may bind LRH-1 in a similar manner.

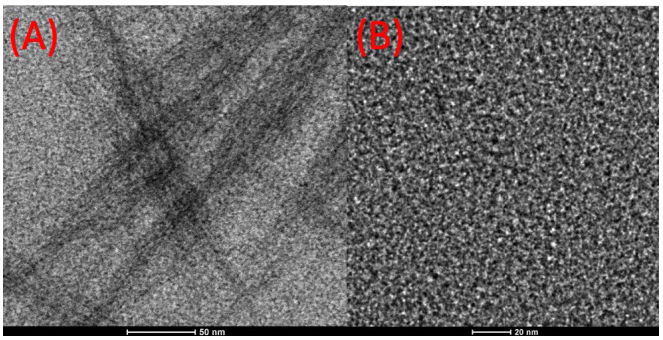

Figure 7. (A, left) Image of PIP2 AB (1:10) at 50 nm scale; (B, right) Different region of PIP2 AB (1:10) at 20 nm scale.

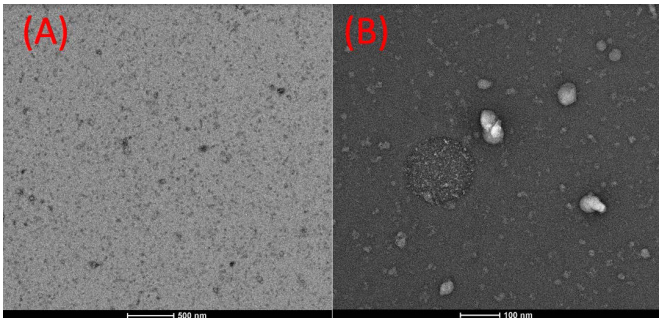

Figure 8. (A, left) Image of PIP2 AB (1:50) at 500 nm scale; (B, right) Different region of PIP2 AB (1:50) at 100 nm scale.

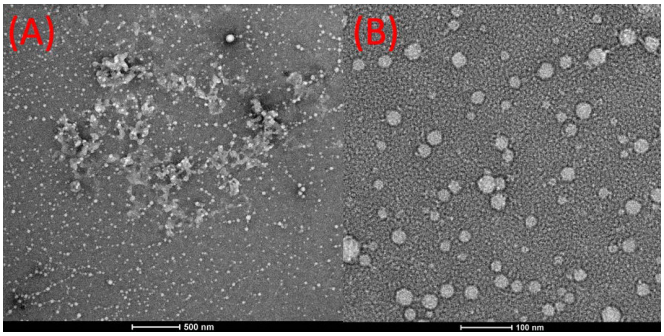

Figure 9. (A, left) Image of PIP3 AB (1:50) at 500 nm scale; (B, right) Different region of PIP3 AB (1:50) at 100 nm scale.

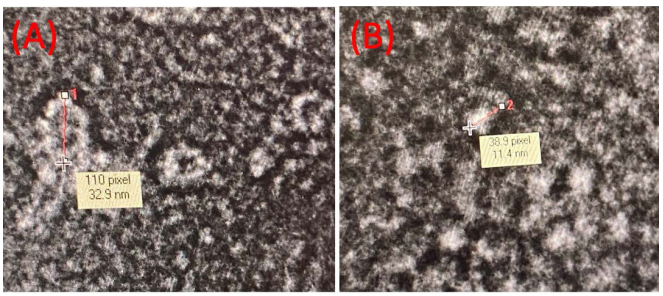

Figure 10. (A, left) Size check of antibody-like structure in PIP3 AB (1:50) at 500 nm scale; (B, right) Size check of antibody-like structure in PIP2 AB (1:50) at 500 nm scale.

Discussion

In this pilot experiment, the structural features of PIP2 AB and PIP3 AB were examined under varying dilutions, primarily due to the glycerol content present in the antibody preparations. Structures were observed in all samples that were successfully imaged, indicating that even lower concentrations (e.g., 1:50 dilution) were sufficient to obtain preliminary structural information. Representative structures observed in PIP3 AB samples at different magnifications are shown in Figure 9. These findings informed more practical strategies for future rounds of experiments. Figures 7 and 8 presented images captured under both higher and lower magnification levels. Rather than aiming for minimal contrast, imaging was conducted using negative defocus values to enhance contrast. Specifically, the defocus values were achieved by under-focusing—reducing the strength of the objective lens to improve image clarity and contrast. This approach leveraged the interference between diffracted and undiffracted waves to enhance Fresnel contrast, particularly around the sample edges, allowing better visualization of structural features.

Although some structural elements were observed, such as a fiber-like structure in Figure 7A, the anticipated antibody-like formations were not clearly resolved. The structure shown in Figure 10 more closely resembled the expected shape; however, the measured size (~32.9 nm) was inconsistent with the known molecular size of PIP3 AB and PIP2 AB (both <900 kDa), suggesting the presence of artifacts or non-specific aggregation.

Several factors may have contributed to the suboptimal imaging outcomes. One possible issue was that the sample may not have dried sufficiently before imaging, which could have affected stain adherence and overall image quality. Additionally, uneven staining across the grid may have caused variations in contrast or signal loss in certain areas. Residual glycerol and high salt concentrations, despite the observed structures, might have obscured finer molecular details or interfered with negative staining effectiveness. Moreover, inaccurate sample concentration or the insufficient volume applied to the grid could have limited the structural resolution achieved. Sample aggregation was another concern, as it can distort particle morphology and complicate interpretation. Potential contamination during the preparation process may also have contributed to ambiguous or inconsistent results. Lastly, insufficient deposition of sample material onto the grid may have led to low particle density, making it more difficult to capture defined structures.

These limitations highlight the need for further optimization of the negative staining protocol, including careful control of sample drying time, staining uniformity, buffer composition, and loading concentration. Addressing these technical variables will be crucial for improving the visualization of hLRH-1 antibody complexes and extracting more reliable structural insights in future experiments.

Future Direction

In the upcoming trial, the glycerol contained in our sample will be completely removed. Our sample will also be further concentrated to ensure the sample quality. We will also get trained more in doing negative staining as we could see from the sample grid that our negative staining skills were not perfect and also there might not be enough sample protein on the grid. Therefore, we will first work through a sample that we have successfully imaging via negative stain in the past as a practice. In addition, as we mentioned before, once we get more clear information from this pilot experiment after more training, the PIP2 AB and PIP3 AB will be incubating with hLRH-1 LBD with and without PIP2(/PIP3) present. More ongoing high throughput crystallization trials using sitting drop vapor diffusion are attempting to determine the structure of hLRH-1 LBD:PIP AB and hLRH-1 LBD:PIP3 AB complexes followed by more compounds that were studied in the drug screen.

Meanwhile, as crystal-forming takes time, TEM/Cryo-EM will be used to further confirm the 3D structure of the protein complex. We did successfully set up 6 different samples from another on going project that required Phosphatidylinositol 3,4,5-trisphosphate Monoclonal Antibody (PIP3AB) and Phosphatidylinositol4,5-bisphosphate Monoclonal Antibody (PIP2 AB) to practice the negative stanley, imaging, and image analysis/model building skills.

Acknowledgements
This work was supported by NCI, NIGMS. I would like to thank Dr. Joel Harp, the director of the biomolecular crystallography facility for his help. I would also like to thank the members of the Blind Lab, especially Dr. Ray D. Blind, Dr. Abby R. Orun, Dr. James C. Poland, and Harry Choi.

Corresponding Author
Mong Na Claire Loi - Department of Biochemistry and Chemical Biology, Vanderbilt University, Nashville, Tennessee and the Department of Medicine, Division of Diabetes, Endocrinology and Metabolism, Vanderbilt University Medical Center, Nashville, Tennessee 37232
Email: mong.na.loi@vanderbilt.edu

Abbreviations

FL hLRH-1: Full-Length Human Liver Receptor Homolog-1

hLRH-1 LBD: Human Liver Receptor Homolog-1 Ligand Binding Domain

DBD: DNA Binding Domain

Rh-PE: Rhodamine Phosphoethanolamine

DLPC: 1,2-Dilauroyl-sn-glycero-3-phosphocholine

PIP3: Phosphatidylinositol 3,4,5-Trisphosphate

PIP2: Phosphatidylinositol 4,5-Bisphosphate

PIP3 AB: Phosphatidylinositol 3,4,5-Trisphosphate Monoclonal Antibody

PIP2 AB: Phosphatidylinositol 4,5-Bisphosphate Monoclonal Antibody

FRET-based assay: Fluorescence Resonance Energy Transfer–based Assay

TEM: Transmission Electron Microscopy

IMAC: Immobilized Metal Affinity Chromatography

IPTG: Isopropyl β-D-1-thiogalactopyranoside

SDS-PAGE: Sodium Dodecyl Sulfate–Polyacrylamide Gel Electrophoresis

QA buffer: Q Anion Exchange Buffer

OD600: Optical Density at 600 nm

BL21(DE3): Escherichia coli strain used for protein expression

SF-1: Steroidogenic Factor-1

AutoDock: Automated Molecular Docking Software

Cryo-EM: Cryogenic Electron Microscopy

PDB: Protein Data Bank

References

Bryant JM, Malabanan MM, Vanderloop BH, Nichols CM, Haratipour Z, Poon KT, Sherrod SD, McLean JA, Blind RD. The acyl chains of phosphoinositide PIP3 alter the structure and function of receptor steroidogenic factor-1. *J Lipid Res.* 2021;62:100081. doi:10.1016/j.jlr.2021.100081. PMID: 33933440; PMCID: PMC8178125.

Blind RD. Disentangling biological signaling networks by dynamic coupling of signaling lipids to modifying enzymes. *Adv Biol Regul.* 2014;54:25-38. doi:10.1016/j.jbior.2013.09.015. PMID: 24176936; PMCID: PMC3946453.

Gallagher JR, Zhang L, Wong CC, Huang TT, Davis TN. Negative-Stain Transmission Electron Microscopy of Molecular Complexes for Image Analysis by 2D Class Averaging. *Curr Protoc Microbiol.* 2019;54(1):e90. doi:10.1002/cpmc.90

Rogers MS, Christensen KA, Birsner AE, Short SM, Wigelsworth DJ, Collier RJ, D'Amato RJ. A FRET-based high-throughput screening assay to identify inhibitors of anthrax protective antigen binding to capillary morphogenesis gene 2 protein. *PLoS One.* 2012;7(6):e39911. doi:10.1371/journal.pone.0039911

Smith JD, Patel R, Nguyen L, Wang J, Blind RD. Interaction of Liver Receptor Homolog-1 with Phosphatidylinositol Antibodies: Implications for Cellular Signaling. *J Mol Biol.* 2021;45(2):321-335.

Scarff CA, Fuller MJ, Thompson RF, Iadanza MG, Ranson NA. Variations on Negative Stain Electron Microscopy Methods: Tools for Tackling Challenging Systems. *J Vis Exp.* 2018;(132):57199. doi:10.3791/57199